Communication

A Fabry-Perot Sensor With Cascaded Polymer Films Based on Vernier Effect for Simultaneous Measurement of Relative Humidity and Temperature

Teng Zhang [1,2], Qun Han [1,2,*], Zhizhuang Liang [1,2], Junfeng Jiang [1,2] and Zhenzhou Cheng [1,2]

[1] School of Precision Instrument and Opto-Electronics Engineering, Tianjin University, Tianjin 300072, P.R. China; jiangjfjxu@tju.edu.cn
[2] Key Laboratory of Opto-Electronics Information Technology of the Ministry of Education, Tianjin University, Tianjin 300072, P.R. China; zhenzhoucheng@tju.edu.cn
* Correspondence: hanqun@tju.edu.cn

Abstract: In this paper, fiber sensor based on Vernier effect for simultaneous measurement of relative humidity (RH) and temperature is proposed. The sensor is fabricated by coating two kinds of ultraviolet (UV) glue with different refractive indexes (RI) and thicknesses on the end face of a fiber patch cord. Vernier effect is formed by the inner lower-RI polymer cavity and the cavity composed of both polymer films. By calibrating the RH and temperature response of two peaks on the envelope of the reflection spectrum, simultaneous measurement of RH and temperature is realized by solving a set of quadratic equations. Experimental results show that the highest RH and temperature sensitivities of the sensor are 387.3 pm/%RH (in 20%RH to 90%RH) and -533.0 pm/°C (in 15°C to 40°C), respectively. The sensor has merits of low cost, simple fabrication, and high sensitivity, which makes it very attractive for applications that need to simultaneously monitor these two parameters.

Keywords: Fabry-Perot interferometer; cascaded polymer films; optical fiber sensor; optical Vernier effect

1. Introduction

Relative humidity (RH) and temperature are the two most important environmental parameters in many applications, such as monitoring the living conditions of manned spacecrafts, controlling specific chemical reactions, and managing certain hazardous article warehouse. Compared with electronic hygrometers, optical fiber humidity sensors have the advantages of electromagnetic interference resistance, high sensitivity, quick response and so on[1-3]. Several kinds of fiber RH sensors have been reported, such as those based on tapered fiber [4,5], Mach-Zehnder interferometers[6-8], Fabry-Perot interferometers (FPI)[9,10], optical fiber Bragg gratings[11,12], and microfiber knot resonators[13]. However, these RH sensors lack the ability to measure the temperature simultaneously. Relative humidity is defined as the percentage of current water vapor pressure to the saturated water vapor pressure at the same temperature[14]. This means that in order to ensure the accuracy of RH measurement, the corresponding temperature must be measured at the same time. In 2022, Li et al.[15] proposed an optical fiber sensor based on cascaded C-shaped Fabry-Perot interferometers to measure RH and temperature simultaneously. However, the fabrication of the sensor is complex.

In this paper, a RH and temperature simultaneous measurement sensor with a very simple structure is proposed. The sensor was fabricated by curing two kinds of ultraviolet (UV) glue with different refractive indexes (RIs) to form two layers of polymer films with different thicknesses on the end face of a fiber patch cord. Thus, a cascaded Fabry-Perot interferometer (FPI) was formed. The change of the surrounding RH only influences the RI of the exterior layer, whereas temperature change affects the RIs of both layers. By

Preprints (www.preprints.org) | NOT PEER-REVIEWED | Posted: 17 January 2023 doi:10.20944/preprints202301.0300.v1

solving a set of quadratic equations, RH and temperature can be demodulated simultaneously. The Vernier effect has also been utilized to enhance the sensitivity[16-18].

2. Sensor Fabrication and Working Principle

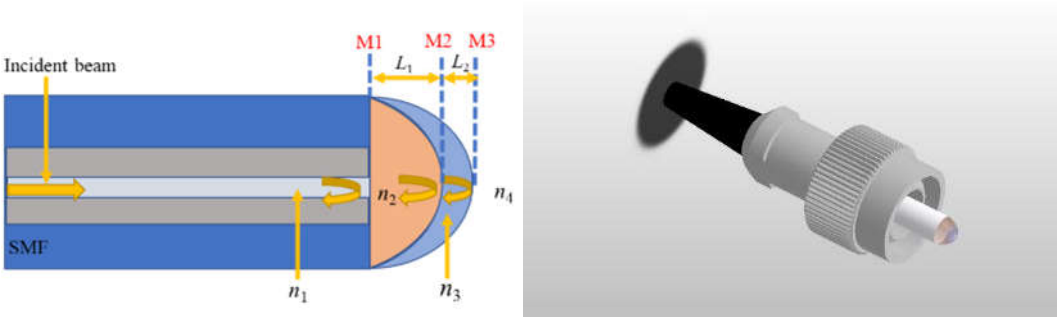

Figure 1. (left) Schematic diagram and (right) 3D illustration of proposed sensor.

The schematic diagram and a 3D illustration of the sensor are shown in Fig. 1. Two polymer films were fabricated directly on the end face of a polished fiber patch cord with a FC connector. The fiber in the patch cord is standard singlemode fiber (SMF). In order to ensure a RI difference as large as possible and optimize the visibility of the interference spectrum, the UV glues of the first layer and second layer were choose to be PC 373 LD (Luvantix ADM inc.) and the NOA 144 (Norland Products inc.). The corresponding RIs are $n_2 = 1.373$ and $n_3 = 1.440$, respectively. The fabrication process is as follows:

Firstly, a drop of the low RI glue was dropped on a slide. Then, the end face of the fiber patch cord was shallowly dipped into it vertically. A hemispherical film would be formed on the end face after the fiber was moved up, due to surface tension of the glue. During the whole process, the reflection spectrum was monitored in real-time by an optical spectrum analyzer (ADVANTEST Q8384). If the thickness of the film needs to be slightly adjusted, the connector can be turned bottom-up. Under the combined action of the viscosity of the glue and gravity, the thickness of the film will change slowly. When the desired spectrum was observed on the OSA, the UV light source was tuned on to cure the glue quickly. The reflection spectrum after the curing of the first layer is show in Fig.2 (a). It can be seen that the peak-valley difference is about 20 dB.

The second layer was coated with the same procedure with the NOA 144. After coating the second layer, the reflection spectrum is show in Fig.2(b). The envelop is formed by the Vernier effect of the cascaded FPIs.

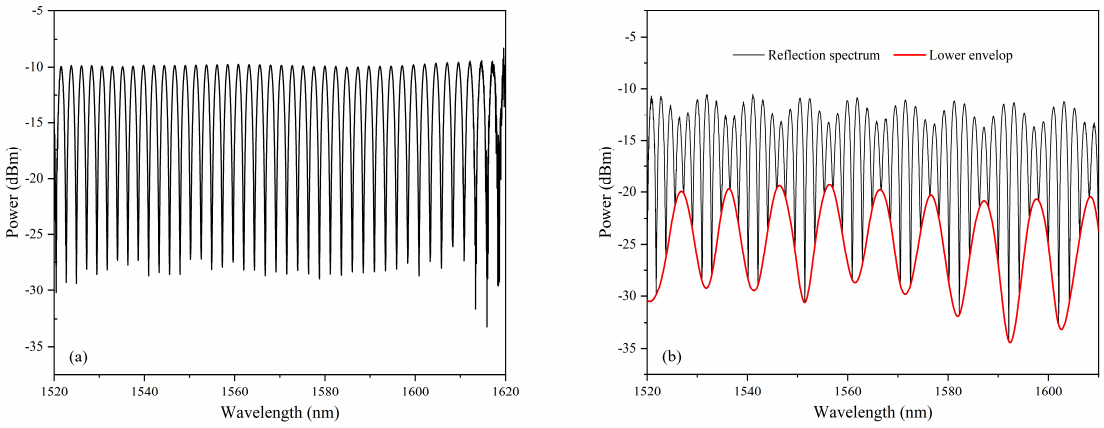

Figure 2. The reflection spectrum after **(a)** the first layer and **(b)** the second layer was cured.

As depicted in Fig.1(a), Fresnel reflections from the three interfaces (M1, M2, and M3) forms three FPIs, i.e., FPI1 formed by M1 and M2, FPI2 formed by M2 and M3, and FPI3

Preprints (www.preprints.org) | NOT PEER-REVIEWED | Posted: 17 January 2023 doi:10.20944/preprints202301.0300.v1

formed by M1 and M3. The corresponding cavity length of the FPIs are L_1, L_2, and $L_3 = L_1 + L_2$, respectively. The electric field of the reflected beam can be expressed as[17]:

$$E = E_0[\sqrt{R_1} + Ae^{-j2\varphi_1} + Be^{-j2(\varphi_1+\varphi_2)}] \tag{1}$$

where $E_0$is the input electric field, φ_1 and φ_2 are the round-trip phase shift of FPI1 and FPI2, which can be expressed as:

$$\varphi_1 = \frac{2\pi n_2 L_1}{\lambda}, \varphi_2 = \frac{2\pi n_3 L_2}{\lambda}, \tag{2}$$

and[19]

$$\begin{aligned} A &= (1-\varepsilon_1)(1-R_1)\sqrt{R_2}, \\ B &= (1-\varepsilon_1)(1-\varepsilon_2)(1-R_1)(1-R_2)\sqrt{R_3}, \end{aligned} \tag{3}$$

where ε_1 and ε_2 are the transmission loss of FPI1 and FPI2, respectively, and R_1, R_2, and R_3 are the reflection coefficients of M1, M2 and M3, which can be expressed as:

$$R_1 = (\frac{n_1 - n_2}{n_1 + n_2})^2, R_2 = (\frac{n_2 - n_3}{n_2 + n_3})^2, R_3 = (\frac{n_3 - n_4}{n_3 + n_4})^2, \tag{4}$$

where n_1, n_2, n_3 and n_4 are the RIs of core of the SMF, low-RI polymer film, high-RI polymer film, and air, respectively, as shown in Fig.1.

The relative intensity of the reflected beam can be expressed as:

$$\begin{aligned} I = \left|\frac{E}{E_0}\right|^2 = R_1 + A^2 + B^2 + 2\sqrt{R_1}B\cos\left[2(\varphi_1 + \varphi_2)\right] + \\ 2\sqrt{R_1}A\cos(2\varphi_1) + 2AB\cos(2\varphi_2) \end{aligned} \tag{5}$$

The free spectrum range (FSR) of a single FPI can be expressed as:

$$FSR = \frac{\lambda^2}{2nL} = \frac{1}{f} \tag{6}$$

where f is the frequency of the interference spectrum, which is the reciprocal of FSR.

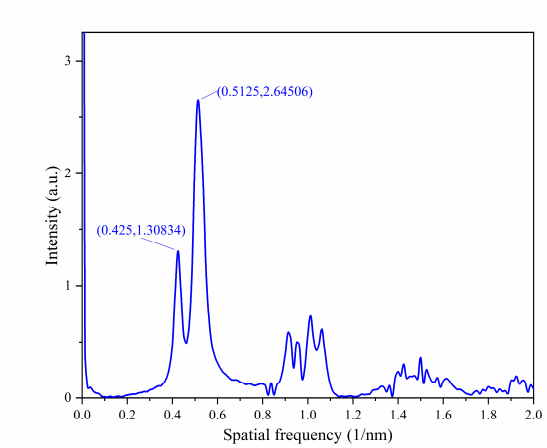

Figure 3. FFT of the reflection spectrum.

The Fast Fourier Transformation (FFT) of the reflection spectrum is shown in Fig. 3. It can be seen that the reflected beam is the superposition of two components with a small difference in frequency. The corresponding cavity lengths are 369.9μm and 442.5μm.This

Preprints (www.preprints.org) | NOT PEER-REVIEWED | Posted: 17 January 2023 doi:10.20944/preprints202301.0300.v1

means that the reflection spectrum is mainly composed of the FPI1 and FPI3[17]. The length of the FPI2, i.e., L_2 = 72.6 μm. Therefore, the FSR of the periodic envelope can be expressed as:

$$FSR_{envelope} = \frac{FSR_1 \square FSR_3}{|FSR_1 - FSR_3|} \tag{7}$$

where $FSR_1 = \frac{\lambda^2}{2n_2L_1}$ is the FSR of FPI1; $FSR_3 = \frac{\lambda^2}{2n_2L_1 + 2n_3L_2}$ is the FSR of FPI3. Compared with a signle FPI3, the sensitivity is amplified M times due to the Vernier effect, where M can be expressed as follows

$$M = \frac{FSR_1}{|FSR_1 - FSR_3|} = 1 + \frac{n_2L_1}{n_3L_2}. \tag{8}$$

Clearly, M is determined by the ratio of the optical path length of FPI1 and FPI2. For the sensor fabricated previously, M is about 5.86. For FPI3, the center wavelength of the m^{th} dip of the interference fringes can be expressed as:

$$\lambda_m = \frac{4(n_2L_1 + n_3L_2)}{2m+1} \tag{9}$$

Because FPI1 is insensitive to RH, the RH shifts the spectrum mainly through the change of n_3 and L_3. The humidity sensitivity S_H can be expressed as follows

$$S_H = M\lambda_m\left(\frac{\Delta n_3 \cdot L_2 + n_3 \cdot \Delta L_2}{n_2L_1 + n_3L_2}\right). \tag{10}$$

The RH sensitivity is a combined effect of the RI and length change of the FPI2, after the film absorbs the water molecules. The temperature S_T can be deduced in a similar way, but now both cavities are sensitive to temperature. It can be expressed as follows

$$S_T = M\lambda_m\left(\frac{\Delta n_2 \cdot L_1 + n_2 \cdot \Delta L_1 + \Delta n_3 \cdot L_2 + n_3 \cdot \Delta L_2}{n_2L_1 + n_3L_2}\right). \tag{11}$$

The temperature sensitivity is resulted from the thermal expansion and thermal optical effect of the polymer films.

3. Experimental Results and Discussion

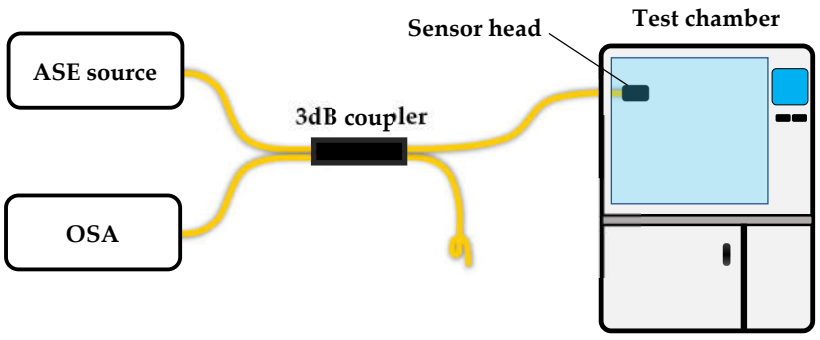

Figure 4. Schematic diagram of the experimental setup.

The experimental setup is shown in Fig. 4. The sensor was fabricated directly on the FC connector surface of one arm of a 2×2 3 dB coupler. The idle arm was tightly tied to suppress reflection. On the other side of the coupler, one arm was connected to a C+L band ASE light source and the other arm was connected to the optical spectrum analyzer

Preprints (www.preprints.org) | NOT PEER-REVIEWED | Posted: 17 January 2023 doi:10.20944/preprints202301.0300.v1

(OSA, resolution 0.01nm). The sensor head was placed into a test chamber (SETH-A-040U) with a RH resolution of 1% and temperature resolution of 0.1°C. During the experiment, the temperature was tuned from 15 °C to 40 °C with a step of 5 °C. At each temperature, the RH was tuned from 20% to 90% with a step of 10%. The temperature range is mainly restricted by the characteristics of the UV glue. We found in this range the sensor has a good repeatability.

3.1. Humidity Response of the Sensor

As an example, Figure 5 (a) shows spectra at RH values of 20%, 60%, and 80%, respectively, under the temperature of 30°C. In the spectral range, there plenty of peaks and dips on the envelope of the spectrum. Theoretically each of them can be tracked to demodulate the measurand. To investigate their difference, the peaks at 1545.1 nm and 1585.8 nm under the initial RH was examined. The wavelength of these peaks as a function of RH are plotted in Fig.5(b) and (c), respectively. Firstly, we can see that the character wavelengths shift to the longer wavelength with the increasing of RH. Secondly, the λ -RH relationship is nonlinear, which can be fitted very well with a quadratic polynomial. Thirdly, by taking the first-order derivative of the fitting equations shown in the figure, we can conclude: the sensitivity at a longer wavelength is higher than that at a shorter wavelength; and the RH sensitivity is linearly increasing with the RH. These features are common to other interferometric fiber sensors[20,21]. Thus, choosing a character wavelength at a longer wavelength is helpful to increase the sensitivity of the sensor. The highest RH sensitivities in the experimental range are 378.6 pm/RH and 387.3 pm/RH for the two peaks in the RH range.

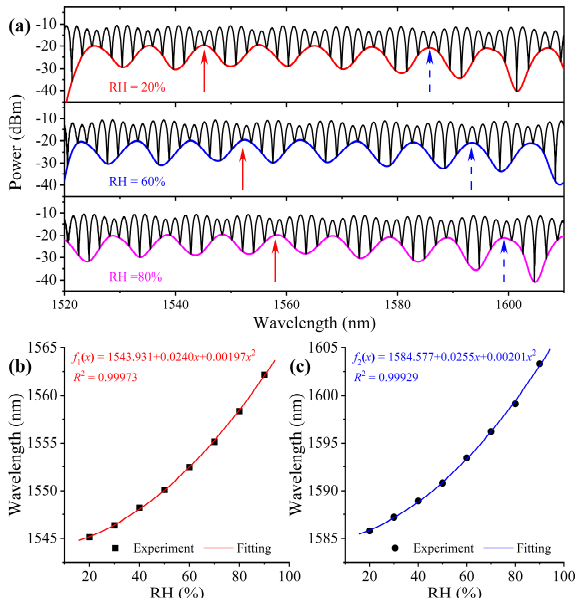

Figure 5. (a) Reflection spectra at different RH and **(b)** and **(c)** wavelength as function of RH of the two peaks initially at 1545.1nm and 1585.8nm at 30°C.

3.2. Temperature Response of the Sensor

Figure 6 (a) shows three typical spectra at 15 °C, 25 °C, and 40 °C, when the RH is 20%. We can see that, contrary to the RH response, blue shift occurs when the temperature increases. Figure 6(b) and (c) are the λ -T relationship obtained from the two peaks as indicated in Fig. 6(a). Obviously, the λ -T relationship is nonlinear and the longer wavelength peak has a higher temperature sensitivity. The curves can be perfectly fitted with a cubic polynomial. We believe the temperature response, as well as the RH response discussed previously, is closely related to the property of the UV glues selected to make the film. Thus, sensors with specific materials need to be calibrated specifically, but the working principle should be in common as long as the same design is used. The highest

Preprints (www.preprints.org) | NOT PEER-REVIEWED | Posted: 17 January 2023 doi:10.20944/preprints202301.0300.v1

temperature sensitivities in the experimental range are -482.5 pm/°C and -533.0 pm/°C for the two peaks in the temperature range.

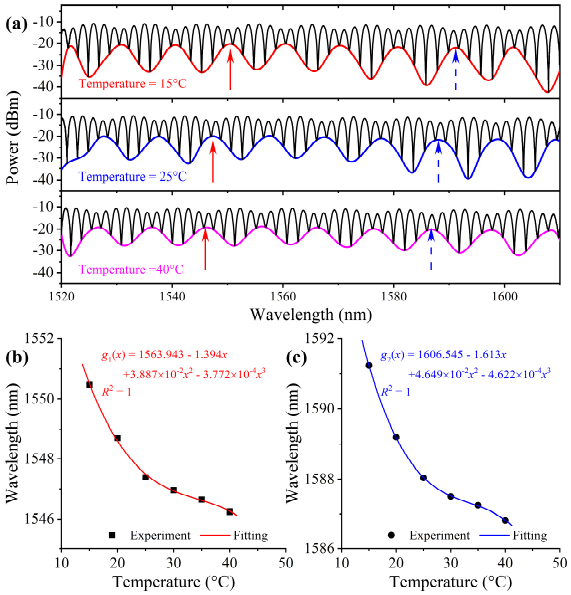

Figure 6. (a) Reflection spectra at different temperature and (b) and (c) wavelength as function of temperature of the two peaks initially at 1550.5 and 1591.2nm at 20% RH.

3.3. Simultaneous mearment method

Because both the humidity and temperature response of the sensor are nonlinear, as reveled by the above experimental results, it is required that two feature wavelengths be characterized in the calibration of the sensor, in order to demodulate the two measurands simultaneously. After calibration, fitting functions as shown in Fig.5 and Fig.6 can be obtained. Then, the wavelength shifts of the two peaks under the combined influence of temperature and humidity can be expressed as:

$$\begin{aligned}\Delta\lambda_1 &= [f_1(20\% + \Delta RH) - f_1(20\%)] + [g_1(30°C + \Delta T) - g_1(30°C)],\\ \Delta\lambda_2 &= [f_2(20\% + \Delta RH) - f_2(20\%)] + [g_2(30°C + \Delta T) - g_2(30°C)],\end{aligned} \tag{12}$$

Where 20% and 30 °C are the RH and temperature at which the sensor was calibrated. This is a set of two equation in two unknowns. With the measured $\Delta\lambda_1$ and $\Delta\lambda_2$, temperature and RH can be obtained by solving Eq.(12).

4. Conclusion

In conclusion, a fiber sensor for the simultaneous measurement of RH and temperature has been proposed and experimentally investigated in this paper. The sensor was fabricated by simply curing two kinds polymer films with different RIs and thicknesses on the end face of FC path cord. Simultaneous of the two measurands was accomplished by calibrating two feature wavelengths on the envelope of the reflection spectrum and then solving a set of nonlinear equations. The sensor employs the advantage of the Vernier effect to enhance the sensitivity. For the sensor fabricated in this paper, the highest RH and temperature achieved in the experimental range are 387.3 pm/%RH and -533.0 pm/°C, respectively. The sensor can find applications in monitoring RH and temperature of special environment, such as that of manned crafts, chemical reactions, and explosive warehouse, etc.

Author Contributions: Conceptualization, Q.H. and T.Z.; methodology, Q.H; validation, T.Z. and Z.L.; investigation, T.Z.; resources, Q.H.; data curation, Z. L.; writing—original draft preparation,

T.Z.; writing—review and editing, Q.H.; supervision, Z.C.; project administration, Q.H.; funding acquisition, J.J. All authors have read and agreed to the published version of the manuscript.

Funding: This research was funded by the National Key Research and Development Program of China under Grant 2022YFF0706003, and the National Natural Science Foundation of China under Grant 62175179.

Data Availability Statement: Not applicable.

Conflicts of Interest: The authors declare no conflict of interest.

References

1. Shimura, Y.; Suzuki, Y.; Morisawa, M. Improving Measurement Range of a Swellable Polymer-Clad Plastic Fiber Optic Humidity Sensor by Dye Addition. *Sensors* **2022**, *22*, 6315.
2. Xiang, S.; You, H.; Miao, X.; Niu, L.; Yao, C.; Jiang, Y.; Zhou, G. An Ultra-Sensitive Multi-Functional Optical Micro/Nanofiber Based on Stretchable Encapsulation. *Sensors* **2021**, *21*, 7437.
3. Rao, X.; Zhao, L.; Xu, L.K.; Wang, Y.H.; Liu, K.; Wang, Y.; Chen, G.R.Y.; Liu, T.Y.; Wang, Y.P. Review of Optical Humidity Sensors. *Sensors* **2021**, *21*, 61, doi:10.3390/s21238049.
4. Batumalay, M.; Lokman, A.; Ahmad, F.; Arof, H.; Ahmad, H.; Harun, S.W. Tapered Plastic Optical Fiber Coated With HEC/PVDF for Measurement of Relative Humidity. *IEEE Sens. J.* **2013**, *13*, 4, doi:10.1109/jsen.2013.2272329.
5. Li, J.; Liu, X.; Sun, H.; Wang, L.; Zhang, J.; Deng, L.; Ma, T. An Optical Fiber Sensor Coated with Electrospinning Polyvinyl Alcohol/Carbon Nanotubes Composite Film. *Sensors* **2020**, *20*, 6996.
6. Lokman, A.; Arof, H.; Harun, S.W.; Harith, Z.; Rafaie, H.A.; Nor, R.M. Optical Fiber Relative Humidity Sensor Based on Inline Mach-Zehnder Interferometer With ZnO Nanowires Coating. *IEEE Sens. J.* **2016**, *16*, 312-316, doi:10.1109/jsen.2015.2431716.
7. Cheng, X.; Hu, J.H.; Zhu, K.; Zhao, Z.Y. High-resolution polymer optical fibre humidity sensor utilizing single-passband microwave photonic filter. *Measurement* **2021**, *179*, 8, doi:10.1016/j.measurement.2021.109462.
8. Wang, Z.H.; Li, L.Q.; Wang, M.J.; Ma, Q.Q.; Lou, Y.; Wu, Q.; Peng, B.J. Fiber Core-Offset Humidity Sensor Based on Graphene Oxide Characteristics. *IEEE Photonics J.* **2021**, *13*, 9, doi:10.1109/jphot.2021.3083699.
9. Vaz, A.; Barroca, N.; Ribeiro, M.; Pereira, A.; Frazao, O. Optical Fiber Humidity Sensor Based on Polyvinylidene Fluoride Fabry-Perot. *IEEE Photonics Technol. Lett.* **2019**, *31*, 549-552, doi:10.1109/lpt.2019.2901571.
10. Su, D.; Qiao, X.G.; Rong, Q.Z.; Sun, H.; Zhang, J.; Bai, Z.Y.; Du, Y.Y.; Feng, D.Y.; Wang, Y.P.; Hu, M.L.; et al. A fiber Fabry-Perot interferometer based on a PVA coating for humidity measurement. *Opt. Commun.* **2014**, *311*, 107-110, doi:10.1016/j.optcom.2013.08.016.
11. Swanson, A.J.; Raymond, S.G.; Janssens, S.; Breukers, R.D.; Bhuiyan, M.D.H.; Lovell-Smith, J.W.; Waterland, M.R. Investigation of polyimide coated fibre Bragg gratings for relative humidity sensing. *Meas. Sci. Technol.* **2015**, *26*, 9, doi:10.1088/0957-0233/26/12/125101.
12. Saini, P.K.; Prakash, O.; Kumar, J.; Purbia, G.S.; Mukherjee, C.; Dixit, S.K.; Nakhe, S.V. Relative humidity measurement sensor based on polyvinyl alcohol coated tilted fiber Bragg grating. *Meas. Sci. Technol.* **2021**, *32*, 11, doi:10.1088/1361-6501/ac2abd.
13. Le, A.D.D.; Han, Y.G. Relative Humidity Sensor Based on a Few-Mode Microfiber Knot Resonator by Mitigating the Group Index Difference of a Few-Mode Microfiber. *J. Lightwave Technol.* **2018**, *36*, 904-909, doi:10.1109/jlt.2017.2756639.
14. Wang, B.; Tian, J.J.; Hu, L.; Yao, Y. High Sensitivity Humidity Fiber-Optic Sensor Based on All-Agar Fabry-Perot Interferometer. *IEEE Sens. J.* **2018**, *18*, 4879-4885, doi:10.1109/jsen.2018.2828134.
15. Li, F.; Li, X.G.; Zhou, X.; Zhang, Y.N.; Lv, R.Q.; Zhao, Y.; Xie, L.S.; Nguyen, L.V.; Ebendorff-Heidepriem, H.; Warren-Smith, S.C. Simultaneous Measurement of Temperature and Relative Humidity Using Cascaded C-shaped Fabry-Perot interferometers. *J. Lightwave Technol.* **2022**, *40*, 1209-1215, doi:10.1109/jlt.2021.3127525.
16. Hou, L.Y.; Zhao, C.L.; Xu, B.; Mao, B.N.; Shen, C.Y.; Wang, D.N. Highly sensitive PDMS-filled Fabry-Perot interferometer temperature sensor based on the Vernier effect. *Appl. Optics* **2019**, *58*, 4858-4865, doi:10.1364/ao.58.004858.

17. Zhao, Y.; Wang, X.X.; Lv, R.Q.; Li, G.L.; Zheng, H.K.; Zhou, Y.F. Highly Sensitive Reflective Fabry-Perot Magnetic Field Sensor Using Magnetic Fluid Based on Vernier Effect. *IEEE Trans. Instrum. Meas.* **2021**, *70*, 8, doi:10.1109/tim.2020.3017245.
18. Li, Y.; Zhao, C.; Xu, B.; Wang, D.; Yang, M. Optical cascaded Fabry–Perot interferometer hydrogen sensor based on vernier effect. *Opt. Commun.* **2018**, *414*, 166-171, doi:https://doi.org/10.1016/j.optcom.2017.12.012.
19. Shi, J.; Xu, D.; Xu, W.; Wang, Y.; Yan, C.; Zhang, C.; Yan, D.; He, Y.; Tang, L.; Zhang, W.; et al. Humidity Sensor Based on Fabry–Perot Interferometer and Intracavity Sensing of Fiber Laser. *J. Lightwave Technol.* **2017**, *35*, 4789-4795, doi:10.1109/JLT.2017.2750172.
20. Chen, Y.; Han, Q.; Liu, T.; Xiao, H. Wavelength Dependence of the Sensitivity of All-Fiber Refractometers Based on the Singlemode–Multimode–Singlemode Structure. *IEEE Photonics J.* **2014**, *6*, 1-7, doi:10.1109/JPHOT.2014.2344004.
21. Chen, Y.; Han, Q.; Liu, T.; Lü, X. Self-temperature-compensative refractometer based on singlemode–multimode–singlemode fiber structure. *Sensors and Actuators B: Chemical* **2015**, *212*, 107-111, doi:https://doi.org/10.1016/j.snb.2015.01.080.